

A theoretical thermodynamic investigation of cascade reactions in dinuclear octa-azacryptates involving carbon dioxide

Morad M. El-Hendawy · Niall J. English ·
Damian A. Mooney

Received: 9 October 2010 / Accepted: 6 January 2011 / Published online: 2 March 2011
© Springer-Verlag 2011

Abstract This paper investigates the thermodynamics of gas-phase CO₂ cascade uptake-reactions in the form of carbonate or monomethylcarbonate anions in the host cavity of various dinuclear octa-azacryptates of *m*-CH₂C₆H₄CH₂ and 2,5-furano-spaced hosts, *L*¹ and *L*² cryptands, using density functional theory (DFT). The cascade process involves two stages, namely the formation of dinuclear cryptate complexes, and the subsequent formation of either μ-carbonato cryptate complexes or μ-monomethylcarbonato cryptates. The geometric and electronic structures were also investigated to determine the parameters that affect the stability of the complexes. Natural bond orbital (NBO) analysis was used to investigate the interactions between the trapped anion and its host. Ion selectivity was studied in terms of the formation of dinuclear cryptate complexes, while the basicity and nucleophilicity of cryptands towards Lewis acids was also studied, and good agreement was found vis-à-vis available experimental data.

Keywords DFT · CO₂ fixation · Dinuclear cryptates · Thermodynamic parameters · NBO analysis

Electronic supplementary material The online version of this article (doi:10.1007/s00894-011-0965-z) contains supplementary material, which is available to authorized users.

M. M. El-Hendawy · N. J. English (✉) · D. A. Mooney
The SFI Strategic Research Cluster in Solar Energy Conversion
and the Center for Synthesis and Chemical Biology,
School of Chemical and Bioprocess Engineering,
University College Dublin,
Belfield,
Dublin 4, Ireland
e-mail: niall.english@ucd.ie

Introduction

Atmospheric CO₂ uptake and conversion into energy-rich organic compounds is catalyzed naturally by the enzyme Rubisco (Ribulose-1,5-biphosphate-carboxylase/oxygenase), which is distributed widely in green plants and algae [1]. As a result of potentially alarming reports linking global warming to the steadily increasing concentration of anthropogenic CO₂ in the atmosphere, there is currently much effort underway to ‘mimic’ CO₂ fixation artificially [2–16]. Despite CO₂ being considered one of the most inexpensive and plentiful sources of carbon, it is also one of the most inaccessible, due in large part to its chemical inertness. Thus, if rendered possible, the chemical activation of CO₂ could help serve to reduce its level in the atmosphere, while at the same time allowing CO₂ to be exploited as a carbon feedstock for the production of useful organic compounds [2].

Many studies refer to the importance of host cavities in transition metal complexes as catalysts in taking up and activating CO₂ from air [3–14]. One such strategy of cryptand complexation was developed by Lehn and co-workers over 30 years ago [17], the central idea of which lies in the replacement of the first solvation shell of a cation by a surrogate shell of a three-dimensional (3D) caged ligand-like “cryptand” to enhance both the thermodynamic and kinetic stability of the product (the so-called “cryptate effect”) [17]. Then, the formed macrocyclic complex can trap an anion like carbonate from solution. This effect underlies the varied applications of cryptands; they can be utilized for detoxification, environmental remediation, hydrometallurgy, etc. [18]. However, polyaza-cryptands constitute good candidates for incorporation into ion-selective membrane responsive to transition or heavy-metal cations, while polyether cryptands are responsive to alkali metal cations [18].

The bis-tren cryptands of interest in this work, L^1 and L^2 , are shown in Fig. 1. These cryptands are octamine cages consisting of two tripodal tetramine sub-units, linked covalently by given spacers ($-\text{CH}_2-\text{CH}_2-$). These ligands are able to bind firstly with two metal ions, then an anion such as carbonate anion, according to a cascade mechanism [5, 9, 19]. In homodimetallic complexes, each metal center (M^{2+}) occupies a tren cavity (i.e., a coordination number of 4). Accordingly, it behaves as a receptor for anions [19], which serve to fill the otherwise empty cavities and adopt their donor atoms for coordination with both metal centers, forming trigonal bipyramidal or octahedral geometry [9]. Recently, dinuclear azacryptates of $m\text{-CH}_2\text{C}_6\text{H}_4\text{CH}_2$ [5, 9] and 2,5-furano-spaced hosts [5], namely L^1 and L^2 (cf. Fig. 1), have shown somewhat different tendencies to catalyze CO_2 -uptake reactions within the sterically protected host cavities that form homodinuclear μ -carbonato cryptates. Although the host molecules L^1 and L^2 exhibit a similar structure, carbonato-complexes of L^1 display further reactivity with primary alcohol-forming carbonate monoesters [5, 9], while those of L^2 do not. The failure of L^2 to do so may lie in the insufficient spacing between the pair of transition metals to accommodate the monomethyl ester [9].

The cascade reaction of CO_2 uptake takes place in two stages:

- (1) Formation of a dinuclear cryptate by encapsulation of two transition metal cations in the host cavity of the cryptand

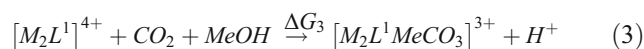
(L). The metal cations of concern here are of the late first-row transition elements (from Co^{2+} to Zn^{2+}):



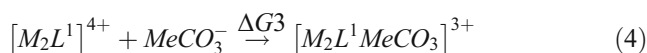
- (2) Encapsulation of an anion in the host cavity of the dinuclear cryptate. Here, the carbonate anion may originate from a pre-formed carbonate or from the atmosphere. In the latter case, CO_2 reacts with the aqueous solution surrounding the dinuclear cryptate and forms CO_3^{2-} . Then the dinuclear cryptate uptakes the CO_3^{2-} anion, forming homodinuclear μ -carbonato cryptates:



It is found that the replacement of the aqueous medium by methanol leads to the direct formation of monomethyl ester only in the case of the cryptand according to reaction given in Eq. 3 [5, 9]:

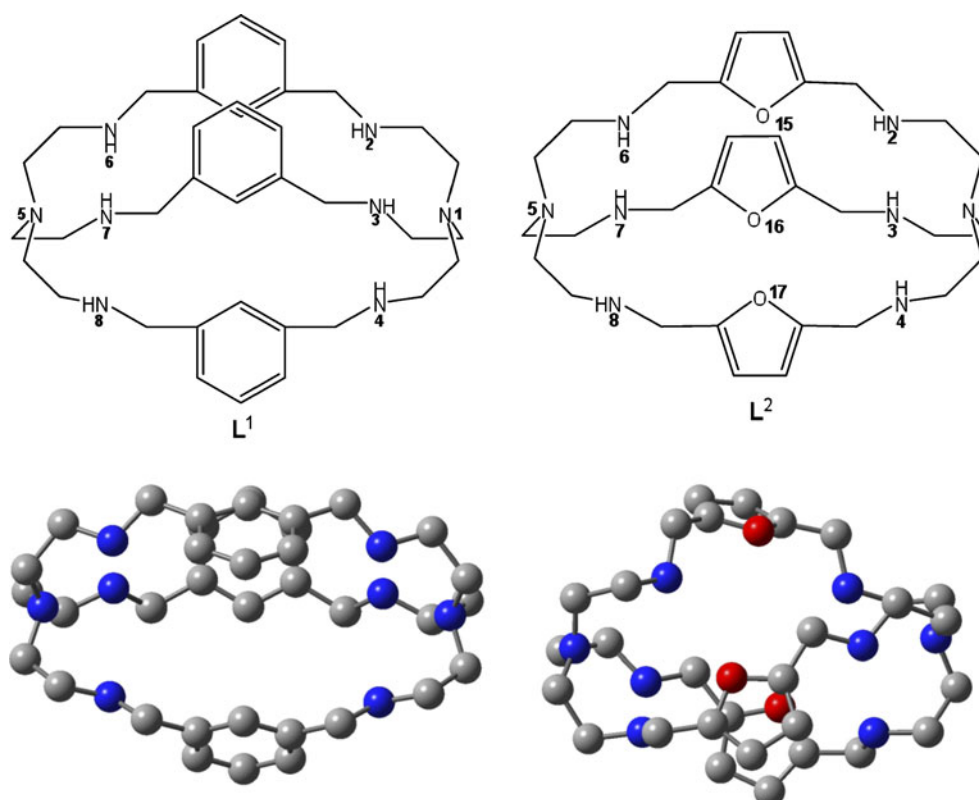


Alternatively, this can be simplified to the overall reaction:



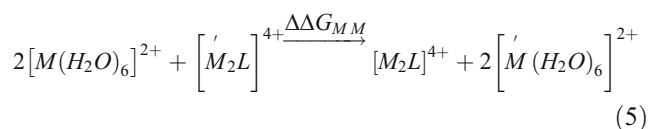
This means that replacement of one H-atom of water by a methyl group (as in methanol) has a positive impact,

Fig. 1 Chemical structures of cryptands L^1 and L^2 and their gas-phase optimized structures calculated using the B3LYP/6-311+G(d,p) approach. Hydrogen atoms are omitted for clarity (see Supplementary Information for positions). Only the labels of key atoms are shown on the chemical structures. *Blue* Nitrogen atoms, *red* oxygen atoms



because one C-atom from CO₂ is added to another C-atom from methanol. This behavior has been reported for other complexes in the literature [14]. This indicates the possibility of the utility of cryptate complexes for the production of chemical feedstock.

The ultimate goal of this work is to provide a quantum-based understanding of the complexation reactions (discussed above) and to also investigate the effects, if any, that the metal ion may have. This is achieved by the calculation of Gibbs free energies and enthalpies of the gas-phase reactions described by the reactions described by Eqs. 1–3. An interesting question to consider is the relative selectivity of the cryptate towards the transition metal ion. These results have a direct impact on the cavity size and reactivity of the formed cryptate towards reaction with anionic substrates. This may be understood by considering the following:



It is expected that because both cryptands have a very similar structure, their stability will be very close. Therefore we have studied their global and local nucleophilicity and basicity to show the affinity of both cryptands towards reaction with a Lewis acid.

Methodology

Single-crystal structures of cryptands and their complexes were obtained from the Cambridge Structural Database (CSD), where available. The referenced sources for the coordinates of cryptands L^1 and L^2 are references [20] and [21]. The CCDC reference numbers of the carbonate cryptate complexes were 181027, 181029, 181031 and 181034 for Cu, Ni, Co and Zn in conjunction with L^1 -based carbonate cryptate complexes, respectively, and 181032 for Co with the L^2 -based complex. Because of the unavailability of X-ray structures of Ni, Cu and Zn cryptates of L^2 , we have employed the results of other experimental analysis tools that suggest that they have similar structures to [CoL²CO₃]²⁺ [9]. Thus, these were derived here from their analogues by replacement of Co atoms with Ni, Cu or Zn atoms. Because of the unavailability of the coordinates of homo-dinuclear cryptates, they were derived from the corresponding carbonate-bridged cryptates by dropping out the carbonate anion in the initial structures. However, the CCDC reference numbers of L^1 -based methylcarbonate-bridged cryptates in the case of Cu, Ni and Zn were 181028, 181030 and 181033, respectively. The initial structure of the Co-derivative was taken from the analogous

Ni form. In this work, all interfering species, such as residual solvents, were removed from the crystal structure before the calculations. Counter-ions were not considered due to computational intractability.

All calculations were performed using the Gaussian 09 suite [22], using density functional theory (DFT) in conjunction with the B3LYP functional [23–25]. Among quantum chemical methods for computational modeling of macrocyclic ligands and their complexes, DFT has been applied successfully to the calculation of the thermodynamic parameters for the cryptate formation reaction [26–28]. Since hydrogen atoms usually have low X-ray scattering factors and, as a result, their coordinates are not generally determined, structures from crystal data were subject to proton optimization at the B3LYP/6-31G(d) level, with the coordinates of heavy atoms fixed. Because the complexes of interest include open shell transition metal cations (Co²⁺, Ni²⁺ and Cu²⁺), they possess a number of different spin states. Therefore, it is necessary to know the energy of these states. The closed-shell singlet and open-shell triplet (quintet and septet if any) states, as well as the antiferromagnetic singlet states, were optimized at either the RB3LYP/6-311+G(d,p) or UB3LYP/6-311+G(d,p) level. Although the energetic differences among these states are small, we found that the antiferromagnetic state is the lowest in energy (cf. Table S1). This result agrees with the magnetic measurement of these complexes [9]. Therefore, we used this state to represent the studied complexes in this paper. However, dinuclear zinc complexes have a closed 3d-shell, thus closed-shell singlet states were used to model these at the RB3LYP/6-311+G(d,p) level. Frequency calculations were carried out to verify that structures were indeed optimized to their energy minima (i.e., without any imaginary frequency components). In addition, natural bond orbital (NBO) analysis was undertaken using the NBO 3.1 program [29], as implemented in Gaussian 09.

Because cryptands act as nucleophilic ligands in the reaction of a Lewis acid (i.e., either hydrogen protons or transition metal cations), global and local nucleophilicities were estimated according to the following procedure. The global nucleophilicity (N) is the reciprocal electrophilicity (ω), which is calculated using the following equation [30]:

$$N = \frac{1}{\omega} \text{ where } \omega = \frac{\mu^2}{2\eta} \quad (6)$$

where μ is the electronic chemical potential and η is the chemical hardness. These two parameters were calculated using the vertical ionization potential and electron affinity; for further details, see [31]. To evaluate the nucleophilic power of the reactive sites within the molecule, a local

nucleophilicity index was evaluated using the following equation [30]:

$$N^-(r) = N^* f_k^- \quad (7)$$

where f_k^- is the Fukui function for electrophilic attack (e.g., Lewis acid) on the nucleophilic sites (e.g., the nitrogen atoms in the cryptand):

$$f_k^- = q_k(N) - q_k(N-1) \quad (8)$$

where $q_k(N)$ and $q_k(N-1)$ are the atomic population of atoms within the molecular species of N and $N-1$ electrons, respectively. This is discussed in further detail in [31].

Results and discussion

Cryptands

Here, we consider the cryptands L^1 and L^2 prior to reaction with the metal ions. The optimized structures of L^1 and L^2 are shown in Fig. 1, together with their molecular structure. Geometry-optimised structural parameters are in good agreement with structural parameters determined by X-ray crystallography (cf. Supplementary Information, Table S2). The RMSD between the theoretical and experimental structures for L^1 and L^2 are small at 0.837 and 0.166 Å, respectively, with most structural deviation arising from the position of the hydrogen atoms.

Table 1 reports the natural population analysis (NPA) and local nucleophilicity of the nitrogen atoms in the cryptands. It is apparent that the charges on the bridgehead nitrogen atoms N1 and N5 are less than those of the other nitrogen atoms. For example, the NPA charge on the tertiary bridgehead nitrogen atoms of L^1 is less than that of the other nitrogen atoms by 12%. This agrees qualitatively with a previous experimental study that investigated the

Table 1 Natural population analysis (NPA) charge (q) and local nucleophilicity (N_k^-) for key atoms in L^1 and L^2

Key site	$(q)_{L^1}$	$(q)_{L^2}$	$(N_k^-)_{L^1}$	$(N_k^-)_{L^2}$
N1	-0.60	-0.59	0.378	0.467
N2	-0.68	-0.68	0.373	0.307
N3	-0.68	-0.71	0.373	0.400
N4	-0.68	-0.68	0.372	0.308
N5	-0.60	-0.59	0.377	0.437
N6	-0.68	-0.69	0.374	0.315
N7	-0.68	-0.71	0.371	0.380
N8	-0.68	-0.68	0.374	0.307
O 11	—	-0.48	—	0.216
O12	—	-0.48	—	0.217
O13	—	-0.48	—	0.215

Table 2 The global nucleophilicity and proton affinity calculated in this work together with the experimentally measured overall basicity

	L^1	L^2
Global nucleophilicity	0.921	0.907
Proton affinity ($-\Delta H$) kcal mol ⁻¹	680	611
Overall basicity ($\sum \log K_i$) ^a	48.3±0.8	44.2±0.8

^aData taken from [21]; ($\sum \log K_i$) is the summation of the measured stepwise protonation constants

basicity of L^1 and L^2 [21]. It was found that, although the ligands have eight potential protonation sites, only six stepwise protonation constants could be determined, which refer to six secondary amines, while the bridgehead amines remained undetectable [21]. The symmetric charge distribution on nitrogen atoms in each tren of L^1 is readily apparent, indicating parallel symmetry in the structure and reactivity. Also, the replacement of phenyl with furanyl rings disrupts this symmetry. Results in Table 1 also suggest that NPA charges and local nucleophilicities on oxygen atoms of L^2 are much less than nitrogen atoms. This reflects the weak tendency for the oxygen atoms in furan rings to react with metal cations, in comparison to nitrogen atoms. This agrees with experimental observations demonstrating that oxygen atoms do not share in the bonding with the metallic centers [21]. However, the local nucleophilicity of N1 and N5 in the cryptand, especially L^2 , is higher than the other atoms, and hence the bonds between these atoms and metal ion would be formed more readily.

Besides the local parameters, the global nucleophilicity and proton affinity of the cryptands were also calculated (Table 2). The proton affinity of a molecule is a measure of its gas-phase basicity, i.e., the energy released in the following reaction:

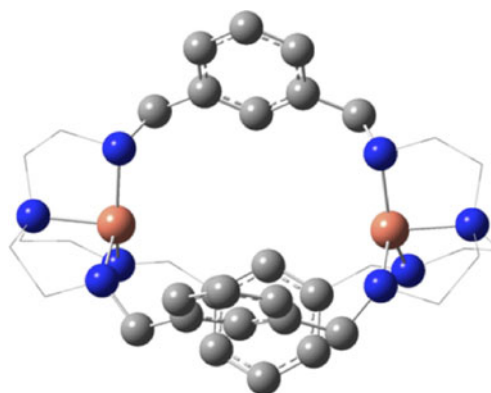


Fig. 2 Optimized geometry of $[Cu_2L^2]^{4+}$; hydrogen atoms are omitted and the carbons atoms around four-fold coordinated metal ions are in stick form for clarification

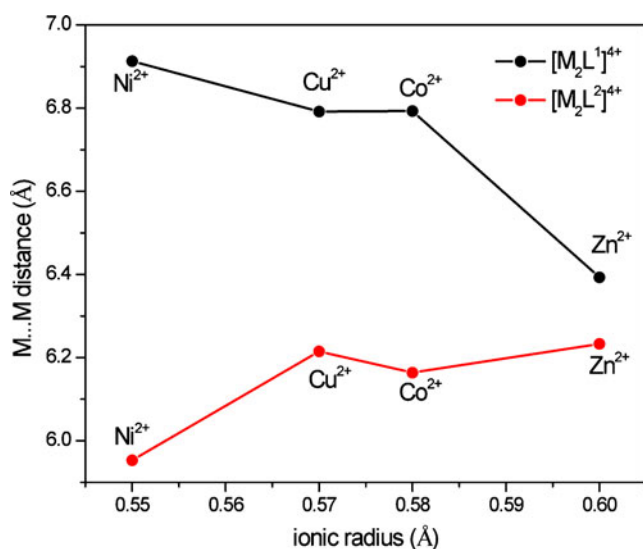


Fig. 3 Dependence of cavity size (M...M distance) (Å) of dimetallic cryptates on the ionic radius of the metal cation (Å)

The proton affinity of the ligand (L) is the negative value of the enthalpy change in the above reaction. Although nucleophilicity and basicity are very similar properties, it is generally accepted that nucleophilicity is a kinetic concept (i.e., characteristic of a rate constant) while basicity is a thermodynamic one [32]. Although basicity is related to the position of an equilibrium reaction with a proton, a good nucleophile is one that forms a new bond rapidly between a base and a proton (H^+) [32]. Table 2 shows the calculated global nucleophilicity and proton affinity together with the overall experimental basicity of L^1 and L^2 . It is clear that L^1 is a better nucleophile and also a better base than L^2 . This may be attributed to the lower basicity of the furanyl rings incorporating L^2 compared to the phenyl ones in L^1 . The ratio between the calculated proton affinities of L^1 and L^2 is 1.02, which is the same the ratio between the overall

Table 4 Relative binding selectivity (kcal mol^{-1}) for L^1 -based and L^2 -based dinuclear cryptates according to the reaction described in Eq. 5

$M^{2+} : M^{2+}$	$(\Delta\Delta G_{MM}')^{L^1}$	$(\Delta\Delta G_{MM}')^{L^2}$
$\text{Cu}^{2+} : \text{Co}^{2+}$	-87	-70
$\text{Cu}^{2+} : \text{Ni}^{2+}$	-11	-51
$\text{Cu}^{2+} : \text{Zn}^{2+}$	-2	-3
$\text{Ni}^{2+} : \text{Co}^{2+}$	-77	-19
$\text{Ni}^{2+} : \text{Zn}^{2+}$	201	240
$\text{Ni}^{2+} : \text{Zn}^{2+}$	277	260

experimental basicities of L^1 and L^2 , lending confidence as to the reliability of our results.

Dinuclear cryptates $[\text{M}_2\text{L}]^{4+}$

Despite there being no published crystallographic structures for the dinuclear cryptates, experimental studies confirm their existence [21, 32, 33]. Therefore, quantum techniques should be able to provide useful insights into the structure of these compounds. The lengths of metal–nitrogen bonds are around 2 Å (cf. Table S3). Meanwhile, Fig. 2 shows the optimized structure of $[\text{Cu}_2\text{L}^1]^{4+}$ as a representative example. As shown, each cation bonds in an enehedral manner into each tren cavity, forming a distorted tetrahedron in which the bridgehead tertiary nitrogen is perpendicular to a triangle of three secondary amino donors. All dinuclear cryptates of interest exhibit the same coordination pattern. However, the distance between the encapsulated metal-pair represents the cavity size in which the carbonate or the monomethylcarbonate anion would be trapped. This depends on the nature of the encapsulated metal cation; for instance, the cavity size in L^2 -based dinuclear cryptates increases as the ionic radius of metal increases. Meanwhile the size in L^1 -based dinuclear cryptates exhibits the reverse

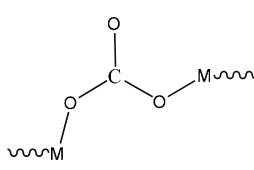
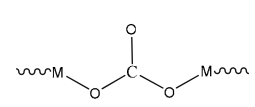
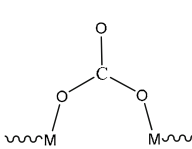
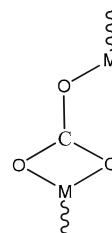
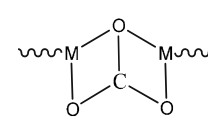
Table 3 Binding Gibbs free energies and enthalpies with $(\Delta G_1^{\text{BSSE}}, \Delta H_1^{\text{BSSE}})$ and without $(\Delta G_1, \Delta H_1)$ basis set superposition errors (BSSE) (kcal mol^{-1}) in the gas phase at 298.15 K for (1) $[\text{M}_2\text{L}^1]^{4+}$ and (2) $[\text{M}_2\text{L}^2]^{4+}$ complexes

	ΔG_1	ΔH_1	BSSE	ΔG_1^{BSSE}	ΔH_1^{BSSE}	Overall stability constant
(1)						
Co^{2+}	-467	-492	6.03	-460	-486	13.56 ^a
Ni^{2+}	-513	-531	9.48	-495	-523	—
Cu^{2+}	-567	-593	5.67	-562	-588	26.20 ^a
Zn^{2+}	-517	-544	6.68	-510	-537	—
(2)						
Co^{2+}	-458	-489	3.77	-454	-482	9.75±0.06 ^b
Ni^{2+}	-496	-524	7.31	-489	-517	—
Cu^{2+}	-564	-592	1.48	-563	-590	25.38±0.08 ^b
Zn^{2+}	-514	-542	6.9	-507	-535	16.10±0.01 ^b

^a Data from [21]

^b Data from [33]

Table 5 Different coordination modes of carbonate bridge in dinuclear metal complexes

Mode symbol	<i>a</i>	<i>b</i>	<i>c</i>	<i>d</i>	<i>e</i>
Mode structure					
Examples	$[\text{Zn}_2\text{L}^1\text{CO}_3]^{2+}$	$[\text{Co}_2\text{L}^1\text{CO}_3]^{2+}$ $[\text{Cu}_2\text{L}^1\text{CO}_3]^{2+}$ $[\text{Ni}_2\text{L}^1\text{CO}_3]^{2+}$	---	---	$[\text{Co}_2\text{L}^2\text{CO}_3]^{2+}$ $[\text{Ni}_2\text{L}^2\text{CO}_3]^{2+}$ $[\text{Cu}_2\text{L}^2\text{CO}_3]^{2+}$ $[\text{Zn}_2\text{L}^2\text{CO}_3]^{2+}$

trend, as shown in Fig. 3. This shows the effect on the chemical structure of the replacement of an *m*-benzene ring by a furanyl one. However, this replacement led to a more compact structure of the host; for instance, the metal–metal distance drops from about 6.6 Å in the case of $[\text{M}_2\text{L}^1]^{4+}$ complexes to about 6.1 Å for $[\text{M}_2\text{L}^2]^{4+}$ complexes.

Nelson and co-workers have attempted to study the binding properties of dinuclear cryptates of L^1 and L^2 with late first-row transition metals from Co^{2+} to Zn^{2+} , but unfortunately L^1 -dinuclear complexation was not observed, except in the case of Cu^{2+} [21]. This contrasts with other studies that confirm the formation of $[\text{Co}_2\text{L}^1]^{4+}$ [33] and $[\text{Ni}_2\text{L}^1]^{4+}$ [34]. It was also found that L^2 generally forms dinuclear cryptates with all transition metals of interest

except in the case of Co^{2+} [21]. As a result, there is no complete picture of the binding properties of these cryptands with transition metal cations. In order to elucidate this matter, we have calculated the Gibbs free energy and enthalpy changes for the complexation reactions in the gas phase at standard conditions according to reaction given in Eq. 1.

There are three approaches for the calculation of thermodynamic parameters of metal-ligand complexation reactions in the gas phase. The first is to consider the bare metal according to reaction given in Eq. 1, and this is the most popular [26]. The second considers a solvated metal cluster, such as hexa-aqua metal complex $[\text{M}(\text{H}_2\text{O})_6]^{2+}$, instead of the bare metal [27]. The third approach combines

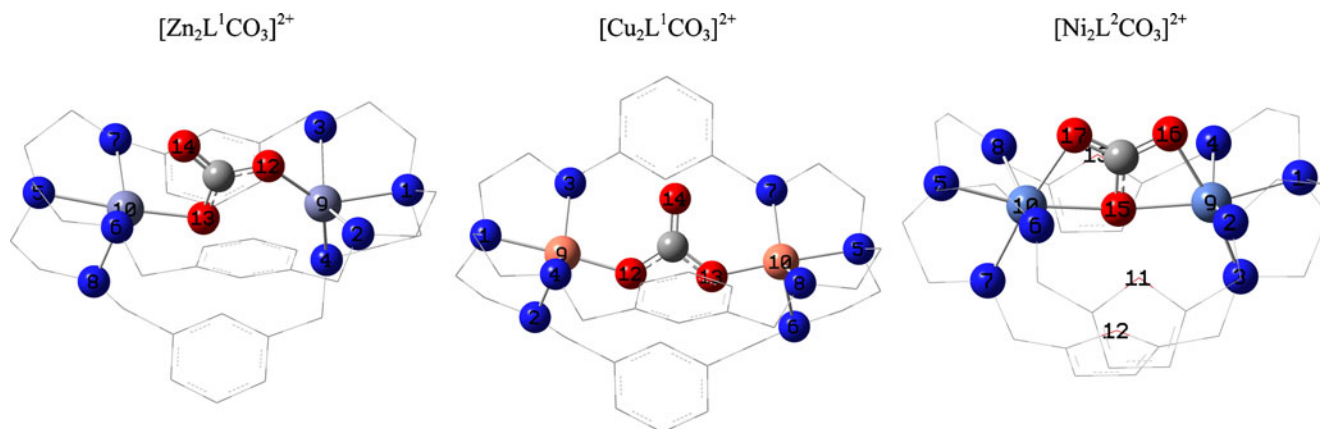


Fig. 4 Optimized geometry of $[\text{Zn}_2\text{L}^1\text{CO}_3]^{2+}$, $[\text{Cu}_2\text{L}^1\text{CO}_3]^{2+}$ and $[\text{Ni}_2\text{L}^2\text{CO}_3]^{2+}$ compounds. The hydrogen and carbons atoms around the coordination center are in stick form for clarification

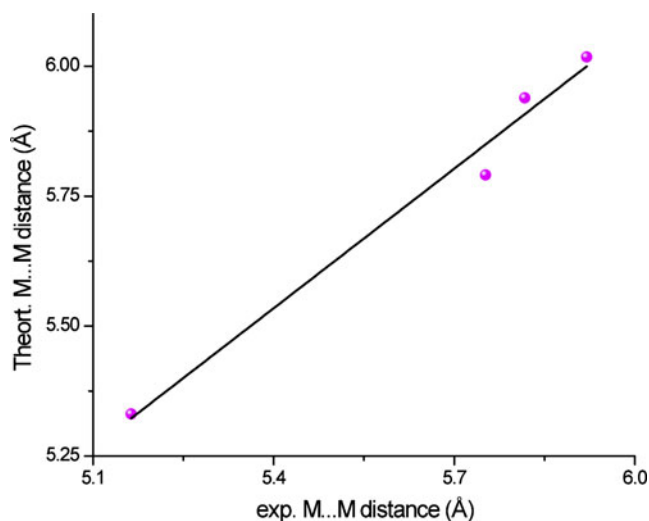
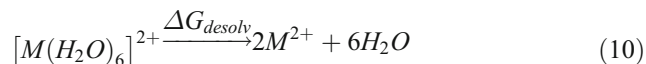


Fig. 5 Correlation plot between experimental and calculated M...M distance (in Å) of $[M_2L^1CO_3]^{2+}$ complexes

the first two [28], wherein the first step is the desolvation of the metal ion according to reaction given in Eq. 10, and the second is the bare metal reaction with the cryptand as in Eq. 1. Then, the free energy of the reaction is the sum of both steps ($\Delta G_1 + \Delta G_{desolv}$).



We calculated the thermodynamic parameters using all three approaches. We found that the first approach works best because it correlates with available experimental data. Therefore, we discuss here only the results of the first approach; the reader is referred to the supplementary information for the other approaches. Table 3 lists the free energy and enthalpy of complexation reactions described by Eq. 1 with and without the basis set superposition errors (BSSE). The BSSE is calculated using the counterpoise method [35]. It is apparent that BSSE does not affect the relative stability of complexes. The stability sequence of dinuclear cryptates has the same order, i.e., $Cu^{2+} > Zn^{2+} > Ni^{2+} > Co^{2+}$, for both ligands. This order agrees with the available experimental results as shown in Table 3. However, as seen, the stability of dinuclear cryptates do not depend greatly on the nature of the cryptand with the same metal. For example, the free energy changes (ΔG_1^{BSSE}) for $[Cu_2L^1]^{4+}$ and $[Cu_2L^2]^{4+}$ are -562 and -563 kcal mol $^{-1}$, respectively. Therefore, we could conclude that the effect of the metal on the stability of dinuclear cryptates is significant.

Because of the previously mentioned applications of cryptands, especially in the extraction of metal ions from an aqueous phase to an apolar organic phase [36], it is important to evaluate the relative binding selectivity to examine the feasibility of extraction. This is the difference

in the free energy change $\Delta\Delta G_{MM'}$, as given by Eq. 5, using the following equations [28]. The experimental relative binding selectivity can be expressed as:

$$\Delta\Delta G_{M,M'}^{exp} = -2.303RT \log \frac{\beta}{\beta'} \quad (11)$$

where β and β' are the overall binding constants. The theoretical relative binding selectivity is calculated as the difference in free energy changes specified in reaction 5:

$$\Delta\Delta G_{M,M'}^{theory} = \Delta G_M - \Delta G_{M'} \quad (12)$$

Table 4 displays the relative binding selectivity between each couple of different metal ions where the first metal ion is solvated with the first solvated shell of water simulated in the aqueous medium and the second metal cation is encapsulated in the cryptand resembling an organic medium. The negative value of the relative binding selectivity is an indication of the feasibility of extraction of the first metal from the aqueous medium. Therefore, the selectivity of L^1 or L^2 towards the Cu^{2+} cation is superior in terms of selectivity vis-à-vis other transition metal cations of interest. This is in agreement with previously reported experiments [21].

Dinuclear carbonato-bridged cryptates $[M_2LCO_3]^{2+}$

It is well-known that the carbonate bridge in dinuclear metal complexes has five different coordination modes depending on the nature of metal and the cavity size [37], as illustrated in Table 5. Because of the high degree of flexibility in the geometry of cryptates, it is important that the techniques used here are able to demonstrate agreement. Actually, DFT-generated geometries of dinuclear carbonato-bridged cryptates exhibit the same coordination modes (**a**, **b**, and **e**) as those obtained from experiment (cf. Table 5).

The optimized geometries of $[Zn_2L^1CO_3]^{2+}$, $[Cu_2L^1CO_3]^{2+}$ and $[Ni_2L^2CO_3]^{2+}$ are shown in Fig. 4 as representative examples for coordination modes of **a**, **b**, and **e**, respectively. Complexes with mode **b** have a trigonal-bipyramidal structure for each metallic center, where the bridgehead nitrogen and one oxygen donor are orthogonal on the face of triangle for which the positions of N2, N3 and N4 constitute its corners. The situation is different in the case of $[Zn_2L^1CO_3]^{2+}$ (mode **a**). While the Zn9 atom embeds in a trigonal-bipyramid arrangement, Zn10 is embedded in a square-pyramid structure. Complexes with mode **e** have distorted octahedral geometries around each metallic center. For example, the Ni9 center in $[Ni_2L^2CO_3]^{2+}$ is embedded in an octahedral motif in which the N2 and N4 positions are semi-orthogonal on a square planar geometry consisting of O12,

Table 6 Binding Gibbs free energies and enthalpies with (ΔG_2^{BSSE} , ΔH_2^{BSSE}) and without (ΔG_2 , ΔH_2) BSSE (kcal mol⁻¹) in gas phase at 298.15 K together with M...M distance (experimental value inbrackets) (Å) and ionic radius of metal cation (Å) for (1) $[\text{M}_2\text{L}^1\text{CO}_3]^{2+}$ and (2) $[\text{M}_2\text{L}^2\text{CO}_3]^{2+}$ complexes

(1)	ΔG_2	ΔH_2	BSSE	ΔG_2^{BSSE}	ΔH_2^{BSSE}	M...M distance	Ionic radius
Co ²⁺	-632	-646	27.36	-605	-619	5.817 (5.939)	0.67
Ni ²⁺	-606	-619	25.66	-580	-593	5.920 (6.018)	0.63
Cu ²⁺	-624	-640	28.87	-595	-611	5.752 (5.791)	0.65
Zn ²⁺	-624	-636	22.76	-601	-613	5.163 (5.331)	0.68
(2)	ΔG_2	ΔH_2	BSSE	ΔG_2^{BSSE}	ΔH_2^{BSSE}	M...M distance	Ionic radius
Co ²⁺	-665	-682	25.83	-639	-656	4.406 (4.292)	0.65
Ni ²⁺	-683	-699	25.66	-657	-674	4.427	0.69
Cu ²⁺	-636	-649	27.80	-608	-621	4.336	0.73
Zn ²⁺	-639	-650	23.55	-616	-627	4.429	0.74

O14, N1 and N3 atoms. In such cases, the carbonate anion acts as a bidentate ligand, the center of which may confer extra stability to the complex compared to those of the other modes. However, the other calculated structural parameters, such as bond length and angle, are in satisfactory agreement with the corresponding published X-ray parameters (cf. Tables S5 and S6). The average percentage errors in bond lengths between these calculations and available X-ray data were 0.86%, 0.65%, 1.12% and 0.96% for Co²⁺, Ni²⁺, Cu²⁺ and Zn²⁺ L¹-based -carbonato cryptates, respectively. For the case of dicobalt-carbonato cryptate (the only one for which experimental structural data is available), the average errors in bond lengths were 1.60%. In terms of critical angles, calculated percentage errors were 3.46%, 5.14%, 1.50% and 6.75% for Co²⁺, Ni²⁺, Cu²⁺ and Zn²⁺ L¹-based -carbonato cryptates, respectively. Again, for the case of dicobalt -carbonato cryptates (the only one for which experimental structural data is available), the average errors in angles were 0.92%. At this point, structural replication was deemed to be of sufficient quality to proceed. An example of the utility of

the techniques used here is the good correlation between the experimental and calculated metal–metal distance of $[\text{M}_2\text{L}^1\text{CO}_3]^{2+}$ (cf. Fig. 5). Another interesting observation is the shortening M...M distance in $[\text{M}_2\text{L}^2\text{CO}_3]^{2+}$ compared to $[\text{M}_2\text{L}^1\text{CO}_3]^{2+}$, which yields more compact structures. For example, while the M...M distance in $[\text{M}_2\text{L}^1]^{4+}$ and $[\text{M}_2\text{L}^2]^{4+}$ complexes hovers around 6.6 and 6.1 Å, the encapsulation of CO₃²⁻ anion in these complexes serves to reduce these to about 5.5 and 4.4 Å, respectively. This is attributed to the arrangement of the carbonate anion (mode e) which interacts with each metallic center as a bidentate ligand. In such cases, the negative carbonate anion attracts two positive centers, leading to a more compact structure. However, the greater drop in M...M distance in the case of the $[\text{M}_2\text{L}^2\text{CO}_3]^{2+}$ complexes is ascribed to the use of the CO₃²⁻ anion to its bidentate character in the interaction with the two positive centers. These observations agree with previous experimental results [9].

It is noteworthy that, compared to L¹-based complexes, the binding of the CO₃²⁻ anion with L²-based complexes is

Table 7 Second-order perturbation interaction energies [E(2)] of $[\text{M}_2\text{L}^1\text{CO}_3]^{2+}$ complexes (kcal mol⁻¹) together with the orbital population of the metal cation given by electrons

Donor → Acceptor	Co ²⁺	Ni ²⁺	Cu ²⁺	Zn ²⁺
LP(O12) → LP*(M9)	63.83	63.50	37.80	47.75
LP(O13) → LP*(M10)	34.20	32.00	45.50	33.53
LP(O14) → LP*(M9)	5.00	6.00	4.00	6.01
LP(O14) → LP*(M10)	4.00	6.00	4.00	2.67
BD(C11-O12) → LP*(M9)	8.00	8.00	6.20	6.6
BD(C11-O13) → LP*(M10)	6.00	7.00	6.00	5.00
BD(C11-O14) → LP*(M9)	5.00	7.50	3.01	4.53
BD(C11-O14) → LP*(M10)	5.00	7.00	—	2.35
$\sum E^{(2)}_{\text{donor} \rightarrow \text{acceptor}}$	131.03	137.00	106.51	108.44
Average population of M ²⁺	4s (0.23)	4s (0.27)	4s (0.25)	4s (0.35)
	3d (7.71)	3d (8.66)	3d (9.51)	3d (9.99)

Table 8 Second-order perturbation interaction energies $E(2)$ of $[M_2L^2CO_3]^{2+}$ complexes (kcal mol⁻¹) together with the orbital population of the metal cation given by electrons

Donor → Acceptor	Co ²⁺	Ni ²⁺	Cu ²⁺	Zn ²⁺
LP(O12) → LP*(M9)	46.76	46.36	14.83	45.14
LP(O13) → LP*(M10)	23.00	28.70	29.37	40.99
LP(O14) → LP*(M9)	26.35	20.33	19.60	2.86
LP(O14) → LP*(M10)	22.00	28.89	17.64	10.00
BD(C11-O12) → LP*(M9)	-7.00	9.50	11.10	4.1
BD(C11-O13) → LP*(M10)	10.00	9.50	4.00	4.60
BD(C11-O14) → LP*(M9)	8.50	3.20	5.11	3.1
BD(C11-O14) → LP*(M10)	5.70	7.20	6.90	3.10
$\sum E^{(2)}_{donor \rightarrow acceptor}$	142.31	153.68	108.55	113.09
Average population of M ²⁺	4s (0.23)	4s (0.27)	4s (0.25)	4s (0.35)
	3d (7.71)	3d (8.66)	3d (9.51)	3d (9.99)

thermodynamically favorable, where the bidentate bonding of carbonate anions with each metallic center in the latter case confers extra stability. However, the stability sequence of dinuclear carbonato-bridged cryptates depends on the binding mode of the carbonate anion (cf. Table 6). For instance, the stability sequence of $[M_2L^1CO_3]^{2+}$ complexes is $Co^{2+} > Zn^{2+} > Cu^{2+} > Ni^{2+}$, while for $[M_2L^2CO_3]^{2+}$ complexes, it is $Ni^{2+} > Co^{2+} > Zn^{2+} > Cu^{2+}$. However, BSSE is important in defining the relative stability among $[M_2L^1CO_3]^{2+}$ complexes. For example, the ΔG_2 values for Cu and Zn-complexes are equal at -624 kcal mol⁻¹, but by considering the BSSE, their ΔG_2^{BSSE} values became -595 and -601 kcal mol⁻¹, respectively. There is no clear-cut relationship between the stability of the complex and the cavity size or ionic radius, but they have an effect. For example, on going from Ni to Zn complexes of $[M_2L^1CO_3]^{2+}$, the ΔG_2^{BSSE} value increases by decreasing the M...M distance and increasing the ionic radius of the metal.

The orbital bonding interactions between metal ions and carbonate anion can be examined by the NBO method [38]. The second-order perturbation energy, $E(2)$, arises between the filled molecular orbital as a donor (i) and the neighboring empty molecular orbitals as acceptor (j). $E(2)$, termed the stabilization energy associated with the delocalization occurring between the donor NBO (i) and the acceptor NBO (j) – 2e stabilization, can be estimated from the following equation:

$$E(2) = \Delta E_{ij} = q_i F^2(i, j) / (\varepsilon_j - \varepsilon_i) \quad (13)$$

where q_i is the i -th donor orbital occupancy, ε_i and ε_j are the diagonal elements (orbital energies) and $F(i, j)$ is the off-diagonal NBO Fock matrix element [38]. As a rule, the greater the value of $E(2)$, the stronger the interaction between a donor NBO and an acceptor NBO. Therefore, $E(2)$ is used to assign and evaluate orbital contributions for stabilizing the complex structures under investigation. Tables 7 and 8 show the $E(2)$ of μ -carbonato cryptate

complexes. In NBO analysis, the NBOs are defined for each covalent bond, lone pair and anti-bonding orbital. Among the possible interactions between each two NBOs, the interaction between the lone pair of the O atom of the carbonate anion and the 3d-antibonding orbital contribute significantly to the stabilization of the complex. The summation of $E(2)$, namely $\sum E^{(2)}_{donor \rightarrow acceptor}$ [39], gives a good correlation with the stability of complex. It is apparent that $\sum E^{(2)}_{donor \rightarrow acceptor}$ is larger for $[M_2L^2CO_3]^{2+}$ complexes than for $[M_2L^1CO_3]^{2+}$ ones, which confirms the bidentate action of carbonate anions for adding extra stability to the former.

Dinuclear μ -monomethylcarbonato cryptates $[M_2L^1MeCO_3]^{3+}$

It is well known that the reaction of CO₂ with hydroxide to generate bicarbonate or carbonate ions is extremely slow in the absence of a catalyst. However, it was reported that dinuclear transition metal complexes are able to uptake

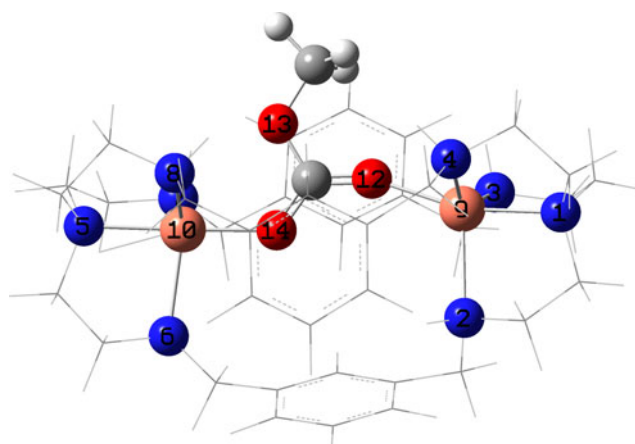
**Fig. 6** Syn-anti μ - η_1 , η_2 arrangement of monomethylcarbonate arrangement within the host cavity of $[Cu_2L^1MeCO_3]^{3+}$

Table 9 Binding Gibbs free energies and enthalpies with (ΔG_3^{BSSE} , ΔH_3^{BSSE}) and without (ΔG_3 , ΔH_3) (kcal mol⁻¹) in gas phase at 298.15 K for $[\text{M}_2\text{L}^1\text{MeCO}_3]^{3+}$ complexes together

	ΔG_3	ΔH_3	BSSE	ΔG_3^{BSSE}	ΔH_3^{BSSE}	M...M distance	Ionic radius
Co ²⁺	-271	-301	6.05	-264	-295	5.591	0.67
Ni ²⁺	-305	-334	6.47	-298	-327	5.648 (5.629)	0.63
Cu ²⁺	-342	-379	5.73	-336	-373	5.667 (5.655)	0.65
Zn ²⁺	-307	-335	6.62	-299	-328	5.888 (5.982)	0.68

with M...M distance (experimental value in brackets) (Å) and ionic radius of metal cation (Å)

atmospheric CO₂ and then catalyze it to form carbonate or bicarbonate [13, 40, 41]. Under ambient atmospheric conditions, the dimetallic cryptates of L¹ form methylcarbonato-bridged cryptates in methanolic solution [9]. The forming of such compounds is considered evidence of the ability of dinuclear cryptates to activate CO₂ and increase the number of carbon atoms by reaction with methanol. This would be considered highly beneficial for producing chemical feedstock compounds.

In this work, the geometries of all methylcarbonato-bridged cryptates of L¹ were optimized using the B3LYP/6-311+G(d,p) method based on the available X-ray coordinates [9]. The calculation showed that the antiferromagnetic species have the lowest energies, which agrees with the experimental finding [9]. The monomethylcarbonate fragment has a syn-anti μ - η_1 , η_2 arrangement within the host cavity of the dinuclear cryptates (see Fig. 6 as a representative example). Table S7 lists some selected bond length and bond angles together with the corresponding X-ray data, if available; it is apparent that there is general agreement with those of the crystal structures. The average percentage errors in bond lengths between these calculations and available X-ray data were 1.20%, 2.26% and 0.79% for Ni²⁺, Cu²⁺ and Zn²⁺, respectively, while the average respective percentage errors in the critical angles, for which the expected flexibility is higher, were 0.15%, 1.1% and 0.25%. An interesting example of this agreement was that both the available experimental and theoretical

metal–metal distances in the series have the same trend: Zn²⁺ > Cu²⁺ > Ni²⁺ > Co²⁺. This order depends on the population of 3d-orbitals of the metal cation. On the other hand, the calculated free energies and enthalpies of binding for $[\text{M}_2\text{L}^1\text{MeCO}_3]^{3+}$ reveal that the strength of binding of dimetallic cryptate with monomethylcarbonate fragment follows the trend: Cu²⁺ > Zn²⁺ \approx Ni²⁺ > Co²⁺, as shown in Table 9; this trend is similar to that of the dinuclear cryptates, but with lower stability. In other words, the encapsulation of the monomethylcarbonate anion destabilizes the monomethylcarbonato cryptates by about 208 kcal mol⁻¹ while the encapsulation of carbonate anion stabilizes it by about 90 kcal mol⁻¹. On the other hand, the negative enthalpy and free energy of the reactions for dinuclear cryptate with the carbonate or monomethylcarbonate anion reflects their exothermic and spontaneous formation, in accord with experimental observations [9].

In order to describe the orbital interaction between the monomethylcarbonate fragment and metallic cations in the dinuclear cryptate, NBO analysis was conducted and the results are presented in Table 10. Here, one can see that the interaction between the lone pairs of oxygen atoms in monomethylcarbonate and the antibonding 3d-orbitals of metal cations contribute significantly to the stabilization of complexes. However, the overall orbital interaction between monomethylcarbonate fragment and the dinuclear cryptate $\sum E^{(2)}_{\text{donor} \rightarrow \text{acceptor}}$ follows the same trend of the overall stability of the complexes. This indicates the

Table 10 Second-order perturbation interaction energies [E(2)] of $[\text{M}_2\text{L}^1\text{MeCO}_3]^{3+}$ complexes (kcal mol⁻¹) together with the orbital population of the metal cation given by electrons

Donor → Acceptor	Co ²⁺	Ni ²⁺	Cu ²⁺	Zn ²⁺
LP(O12) → LP*(M9)	35.08	37.08	39.41	45.14
LP(O13) → LP*(M10)	16.01	19.01	26.84	40.99
LP(O14) → LP*(M9)	—	—	19.32	2.86
LP(O14) → LP*(M10)	13.9	8.46	—	—
BD(C11-O12) → LP*(M9)	—	—	8.7	4.1
BD(C11-O13) → LP*(M10)	14.53	11.53	6.3	3.1
BD(C11-O14) → LP*(M10)	11.13	17.5	9.29	—
$\sum E^{(2)}_{\text{donor} \rightarrow \text{acceptor}}$	90.65	93.58	109.86	96.19
Average population of M2+	4S (0.23) 3d (7.73)	4S (0.23) 3d (8.65)	4S (0.27) 3d (9.51)	4S (0.35) 3d (9.99)

significant dependence of stability of complexes on these orbital interactions.

Conclusions

In conclusion, the DFT geometries of studied cryptands and their complexes are in reasonable agreement with the available X-ray crystallographic data. Also, the calculations have reproduced the arrangement mode of carbonate and monomethylcarbonate anion in the host cavity of dinuclear cryptate. The global nucleophilicity and proton affinity of L^1 cryptand is larger than L^2 towards the Lewis acid which agrees with experimental findings. In addition, L^1 and L^2 -based dinuclear cryptates have comparable stability with the same metallic centers. However, the sequence of stability is the same for both types, $\text{Cu}^{2+} > \text{Zn}^{2+} > \text{Ni}^{2+} > \text{Co}^{2+}$, in accordance with experimental data. It was also found that the mode of arrangement of the carbonate anion in the host cavity of the dinuclear cryptate affects the stability of the complex significantly. The results demonstrate that the reaction of the dinuclear cryptate with carbonate anion is more thermodynamically favorable than that with monomethylcarbonate anion. Finally, the stability of the carbonate or monomethylcarbonate cryptates depends generally on the cavity size where the anionic fragment would be trapped as well as on the ionic radius of the metal cation.

Acknowledgments The authors acknowledge useful conversations with Dr. Grace Morgan. This material is based upon works supported by Science Foundation Ireland (SFI) under Grant No. [07/SRC/B1160]. We also thank SFI and the Irish Center for High-End Computing for the provision of high-performance computing facilities.

References

- Andrews TJ, Lorimer GH (1987) Rubisco: structure, mechanisms and prospects for improvement. In: Hatch MD, Boardman NK (eds) *The biochemistry of plants*, vol 10. Academic, New York, pp 131–218
- Aresta M, Dibenedetto A (2007) Utilization of CO_2 as a chemical feedstock: opportunities and challenges. *Dalton Trans* 28:2975–2992 and references therein
- Kong LY, Zhang ZH, Zhu HF, Kawaguchi H, Okamura T, Doi M, Chu Q, Sun WY, Ueyama N (2005) Copper(II) and zinc(II) complexes can fix atmospheric carbon dioxide. *Angew Chem* 117:4426–4429
- Kersting B (2001) Kohlendioxid-Fixierung an Zweikernkomplexen mit hydrophoben Bindungstaschen. *Angew Chem* 113:4109–4112
- Chen JM, Wei W, Feng XL, Lu TB (2007) CO_2 fixation and transformation by a dinuclear copper cryptate under acidic conditions. *Chem Asian J* 2:710–719
- Kong LY, Zhu HF, Huang YQ, Kawaguchi H, Lu XH, Song Y, Liu GX, Sun WY, Ueyama N (2006) Cadmium(II) and copper(II) complexes with imidazole-containing tripodal polyamine ligands: pH and anion effects on carbon dioxide fixation and assembling. *Inorg Chem* 45:8098–8107
- Verdejo B, Aguilar J, Espana EG, Gavina P, Latorre J, Soriano C, Llinares JM, Domenech A (2006) CO_2 fixation by Cu^{2+} and Zn^{2+} complexes of a terpyridinophane aza receptor. Crystal structures of Cu^{2+} complexes, pH-metric, spectroscopic, and electrochemical studies. *Inorg Chem* 45:3803–3815
- Derossi S, Bond AD, McKenzie CJ, Nelson J (2005) (μ -Bicarbonato- κ 2O, O') [μ -1, 4, 8, 11, 14, 18, 23, 27-octaaza-6, 16, 25(1, 3)-tribenzenabicyclo[9.9.9]nonacosaphane] dicopper(II) triperchlorate acetonitrile solvate. *Acta Crystallogr E* 61:m1379–m1382
- Dussart Y, Harding C, Dalgaard P et al. (2002) Cascade chemistry in azacryptand cages: bridging carbonates and methylcarbonates. *J Chem Soc Dalton Trans* 8:1704–1713
- Bazzicalupi C, Bencini A, Bencini A, Bianchi A, Corana F, Fusi V, Giorgi C, Paoli P, Paoletti P, Valtancoli B, Zanchini C (1996) CO_2 fixation by novel copper(II) and zinc(II) macrocyclic complexes. a solution and solid state study. *Inorg Chem* 35:5540–5548
- Paddock RL, Nguyen ST (2001) Chemical CO_2 fixation: Cr(III) salen complexes as highly efficient catalysts for the coupling of CO_2 and epoxides. *J Am Chem Soc* 123:11498–11499
- Escuer A, Mautner FA, Penalba E, Vicente R (1998) superexchange pathway for the different coordination modes of the carbonate bridge in polynuclear copper(II) compounds. *Inorg Chem* 37:4190–4196
- Kitajima N, Hikichi S, Tanaka M, Moro-oka Y (1993) Fixation of atmospheric CO_2 by a series of hydroxo complexes of divalent metal ions and the implication for the catalytic role of metal ion in carbonic anhydrase. synthesis, characterization, and molecular structure of $[\text{LM}(\text{OH})]_n$ ($n=1$ or 2) and $\text{LM}(\mu\text{-CO}_3)\text{ML}$ ($\text{M}(\text{II})=\text{Mn, Fe, Co, Ni, Cu, Zn}$; $\text{L}=\text{HB}(3,5\text{-iso-Pr}_2\text{pz})_3$). *J Am Chem Soc* 115:5496–5508
- Kato M, Ito T (1986) Syntheses, characterization, and structures of (monomethyl carbonato)-nickel(II), -copper(II), and -cobalt(II) complexes with tetraazacycloalkanes obtained from CO_2 uptake. *Bull Chem Soc Jpn* 59:285–294
- Kato M, Ito T (1985) Syntheses, characterization, and structures of (monomethyl carbonato)nickel(II), -copper(II), and -cobalt(II) complexes with tetraazacycloalkanes obtained from carbon dioxide uptake. *Inorg Chem* 24:504–508
- Kato M, Ito T (1985) Facile carbon dioxide uptake by zinc(II)-tetraazacycloalkane complexes. 2. X-ray structural studies of (μ -monomethyl carbonato)(1, 4, 8, 11-tetraazacyclotetradecane) zinc(II)perchlorate, bis(μ -monomethylcarbonato)tris[(1, 4, 8, 12-tetraazacyclopentadecane)zinc(II)] perchlorate, and (monomethylcarbonato)(1, 4, 8, 11-tetramethyl-1, 4, 8, 11-tetraazacyclotetradecane) zinc(II) perchlorate. *Inorg Chem* 24:509–514
- Lehn JM (1978) Cryptates: inclusion complexes of macropolycyclic receptor molecules. *Pure Appl Chem* 50:871–892, and references therein
- Nelson J, McKee V, Morgan G (1998) Coordination chemistry of azacryptands. In: Karlin KD (ed) *Progress in inorganic chemistry*, vol 47. Wiley, New York, pp 191–192
- Amendola V, Fabbri L, Mangano C, Pallavicini P, Poggi A, Taglietti A (2001) Anion recognition by dimetallic cryptates. *Coord Chem Rev* 219–221:821–837
- Arthurs M, McKee V, Nelson J, Town RM (2001) Chemistry in cages: dinucleating azacryptand hosts and their cation and anion cryptates. *J Chem Educ* 78:1269–1272
- Arnaud-Neu F, Fuangswasdi S, Maubert B, Nelson J, McKee V (2000) Binding properties of octaaminocryptands. *Inorg Chem* 39:573–579
- Frisch MJ, Trucks GW, Schlegel HB et al (2009) GAUSSIAN09, Revision A. 02. Gaussian Inc, Wallingford

23. Becke AD (1993) Density-functional thermochemistry. III. The role of exact exchange. *J Chem Phys* 98:5648–5652
24. Lee C, Yang W, Parr RG (1988) Development of the Colle-Salvetti correlation energy formula into a functional of the electron density. *Phys Rev B* 37:785–789
25. Stevens PJ, Devlin FJ, Chablowski CF, Frisch MJ (1994) Ab initio calculation of vibrational absorption and circular dichroism spectra using density functional force fields. *J Phys Chem* 98:11623–11627
26. Wang X, Wang H, Tan Y (2008) DFT study of the cryptand and benzocryptand and their complexes with alkali metal cations: Li^+ , Na^+ , K^+ . *J Comput Chem* 29:1423–1428
27. Puchta R, Eldik RV (2007) Host–guest complexes of oligopyridine cryptands: prediction of ion selectivity by quantum chemical calculations. *Eur J Inorg Chem* 10:1120–1127
28. Su JW, Burnette RR (2008) First principles investigation of noncovalent complexation: a [2.2.2]-cryptand ion-binding selectivity study. *Chem Phys Chem* 9:1989–1996
29. Glendening ED, Reed AE, Carpenter JE et al. (2003) Program as implemented in the Gaussian 09 package
30. Pratihari S, Roy SJ (2010) Nucleophilicity and site selectivity of commonly used arenes and heteroarenes. *J Org Chem* 75:4957–4963
31. Chattaraj PK, Sarkar U, Roy DR (2006) Electrophilicity index. *Chem Rev* 106:2065–2091
32. Carey FA, Sundberg RJ (1990) *Advanced organic chemistry, Part A. Structure and mechanisms*, 3rd edn. Plenum, New York
33. Menif R, Reibenspies J, Martell AE (1991) Synthesis, protonation constants, and copper(II) and cobalt(II) binding constants of a new octaaza macrobicyclic cryptand: (MX)₃(TREN)₂. Hydroxide and carbonate binding of the dicopper(II) cryptate and crystal structures of the cryptand and of the carbonato-bridged dinuclear copper(II) cryptate. *Inorg Chem* 30:3446–3454
34. Fabbrizzi L, Pallavicini P, Parodi J, Perotti A, Sardone N, Taglietti A (1996) A structurally characterized azidebridged dinuclear nickel(II) cryptate. *Inorg Chim Acta* 244:7–9
35. Boys SF, Bernardi F (1970) The calculation of small molecular interactions by the differences of separate total energies. Some procedures with reduced errors. *Mol Physiol* 19:553–566
36. Khopkar SM (1998) *Basic concepts of analytical chemistry*, 2nd edn. New Age International, New Delhi, pp 112–113
37. Escuer A, Vicente R, Kumar SB, Solans X, Font-Bardía M (1997) A novel tridentate coordination mode for the carbonatonickel system. *J Chem Soc Dalton Trans* 1997:403–408
38. Reed AE, Curtiss LA, Weinhold F (1988) Intermolecular interactions from a natural bond orbital, donor-acceptor viewpoint. *Chem Rev* 88:899–926
39. Kovács A, Nemcsok DS, Kocsis T (2010) Bonding interactions in EDTA complexes. *J Mol Struct THEOCHEM* 950:93–97
40. Palmer DA, van Eldik R (1983) The chemistry of metal carbonato and carbon dioxide complexes. *Chem Rev* 83:651–731
41. Rawle SC, Harding CJ, Moore P et al (1992) Crystal structure of an antiferromagnetically coupled p-carbonato-bridged dinickel(II) complex containing the pendent-arm macrocycle I -(3-dimethylaminopropyl)-1,5,9-triazacyclododecane (L^1); a system which readily sequesters carbon dioxide from air. *J Chem Soc Chem Commun* 1992:1701–1703